Depletion-layer-induced size effects in ferroelectric thin films: A Ginzburg-Landau model study

Nathaniel Ng, Rajeev Ahluwalia, and David J. Srolovitz
Institute of High Performance Computing, Agency for Science, Technology and Research, 1 Fusionopolis Way, 16-16 Connexis, 138632 Singapore

(Received 27 December 2010; revised manuscript received 18 May 2012; published 4 September 2012)

A Ginzburg-Landau model is used to demonstrate how depletion layers give rise to thickness-dependent ferroelectric properties in thin films. It is shown that free charge layers at the film-electrode interface can result in an internal electric field in the bulk of the film even when no external voltage is applied. At high values of the donor dopant density and small thicknesses, this internal electric field can be strong enough to lead to the formation of a domain pattern. This causes a drop in the remnant polarization, a direct demonstration of the important role free charge plays in thin ferroelectric films.

DOI: 10.1103/PhysRevB.86.094104 PACS number(s): 77.80.Dj, 77.80.Fm

I. INTRODUCTION

The progressive miniaturization of devices based upon ferroelectric phenomena has led to an increased interest in size effects in ferroelectric thin films.[1,2] An important issue for device applications is the question of whether a remnant state (i.e., a macroscopically polarized state in the absence of an external electric field) exists within the ferroelectric film as the film thickness is decreased. Such size effects are strongly influenced by the electrical boundary conditions that exist at the ferroelectric-electrode interface.[2] A large body of research on the role of uncompensated bound charges at the electrode[3,4] and associated depolarization fields exists,[5–8] including first-principles work.[9,10] Theory suggests that because of depolarization effects, two critical length scales exist, one below which a single-domain remnant state splits into a multidomain state with 180° domains and the second where ferroelectricity completely disappears.[7,11] However, these analyses of size effects assumed that the ferroelectric is an electrical insulator. In reality, ferroelectrics are usually wide-band-gap semiconductors; this fact can lead to the formation of free charge layers at the ferroelectric-electrode interface. These charge-depleted layers arise from the differences in the work functions between the metal and the ferroelectric,[12] and cause migration of free charges from the ferroelectric into the metal. Depletion layers may also form due to the accumulation of oxygen vacancies at the ferroelectric-electrode interface after repeated cycling of the electric field.[12] Thus, in addition to the traditionally studied bound charge effects, free charge can strongly influence the electrostatic boundary conditions in thin-film devices. How do these charge-depleted layers influence ferroelectric behavior? This question becomes of central importance for thin films where the film thickness becomes comparable to the depletion layer thickness. An understanding of this issue is key, not only from a fundamental standpoint, but for its important implications for device applications.

The role of depletion layers in ferroelectric thin films has received some attention in the literature. Xiao *et al.*[13] demonstrated the formation of a depletion layer based on a Ginzburg-Landau model that incorporated mobile charges. Bratkovsky and Levanyuk[14] showed that depletion charge near the electrode also reduces the ferroelectric/paraelectric transition temperature. Baudry and Tournier[15] and Zubko *et al.*[16] studied the influence of depletion layers on the remnant polarization and hysteresis loops within the Landau theory framework. An analytical study based on a linear approximation to this problem was performed by Tagantsev *et al.*[17] Recently, more sophisticated treatments of the influence of depletion layers on ferroelectrics have been made.[18–20] However, the full implications of the effects of depletion layers on size effects in thin, ferroelectric films remain unexplored. Specifically, the following important issues have not received adequate attention. What is the influence of the depletion layers on the domain patterns as the film thickness is decreased? Do depletion layers have any effect on domain nucleation and growth during switching? In this paper, we employ Ginzburg-Landau theory and phase field simulations to demonstrate that depletion layers have very important consequences for size effects in ferroelectric thin films.

The paper is organized as follows. In Sec. II, we describe the Ginzburg-Landau model for a thin film with depletion layers as well as the kinetic model used to simulate the polarization dynamics. Section III describes the results on the stability of the remnant monodomain states under short-circuit boundary conditions. We analyze these results via a one-dimensional (1D) analytical model in Sec. IV. The role played by depletion layers on polarization switching is discussed in Sec. V. Lastly, we end the paper with a summary and conclusion.

II. GINZBURG-LANDAU MODEL

In the Ginzburg-Landau-Devonshire framework, the total free energy of the system, F_{T}, is

$$F_T = \int d\vec{r}[f_L + f_G + f_{el}], \tag{1}$$

where f_L, f_G, and f_{el} represent the local Landau, gradient, and elastic energy densities, respectively. The Landau energy is obtained from the symmetry-allowed expansion of the free energy as an eighth-order polynomial in the polarization components of $\vec{P}$. Substrate effects are accounted for by assuming a homogeneous in-plane biaxial strain ε that arises from the lattice mismatch between film and substrate. Since our focus is the role of depletion-layer-induced electrostatic effects, we restrict our study to thin films in the region of the phase diagram where they are, effectively, uniaxial ferroelectrics. This is achieved when the compressive misfit

strain is sufficiently large to suppress in-plane ferroelectric polarization.[21] We consider an effective free energy that is nonlinear in P_z (polarization normal to the film); to eighth order in Landau theory,[22] this is expressed as

$$f_L + f_{el} = \tfrac{1}{2}\alpha_1^*\left(P_x^2 + P_y^2\right) + \tfrac{1}{2}\alpha_3^* P_z^2 + \tfrac{1}{4}\alpha_{11}^* P_z^4 + \tfrac{1}{6}\alpha_{111} P_z^6 + \tfrac{1}{8}\alpha_{1111} P_z^8, \quad (2)$$

where $\alpha_1^*,\alpha_3^*,\alpha_{11}^*,\alpha_{111},\alpha_{1111}$ are appropriate material constants.[21] The appropriate contribution from the polarization gradients at domain walls is expressed as

$$f_G = \tfrac{1}{2}K[|\vec{\nabla}P_x|^2 + |\vec{\nabla}P_y|^2 + |\vec{\nabla}P_z|^2]. \quad (3)$$

The electric field, **E**, is obtained by solving Gauss's law,

$$\nabla \cdot \mathbf{D} = \nabla \cdot (-\varepsilon_0 \nabla\phi + \mathbf{P}) = \rho, \quad (4)$$

where

$$\rho(z) = \begin{cases} \rho_0, & z < w \text{ or } d - z < w \\ 0, & \text{otherwise} \end{cases}, \quad (5)$$

the film thickness is d, the depletion layer thickness is w, and $\rho_0 = qN_D$ and N_D are the space charge and donor dopant density. As is well known, the depletion layer thickness depends on the dopant density and the applied and built-in potentials. In the present work, we describe the depletion layer width dependence on the dopant density as $w = \sqrt{2V_{bi}\varepsilon/N_D q} = C/\sqrt{N_D}$,[2,13,16,17,23,24] which has been successfully used to model the semiconducting nature of ferroelectrics in recent works.[16,17,24] Here V_{bi} is the built-in potential, ε is the dielectric constant, and $C = \sqrt{2V_{bi}\varepsilon/q}$ is a constant that represents a property of the ferroelectric-electrode interface. We should remark that while there are more sophisticated calculations which obtain the depletion layer widths in a self-consistent manner,[18] we use the current expression in the present work to simplify the analysis.

We choose parameters appropriate for a $BaTiO_3$ thin film on a $SrRuO_3/SrTiO_3$ substrate with a compressive misfit strain $\varepsilon = -0.022$ (Ref. 7) and gradient coefficient $K = |\alpha_1|\delta^2$, where δ is the smallest length scale resolved in the simulation, which is taken to be $\delta = 1$ nm in the present simulations. Note that we have not included a background dielectric permittivity of the ferroelectric in Eq. (4).[25] This common assumption[13,15,16] is reasonable here since the background dielectric constant is usually much smaller than the dielectric constant of the ferroelectric. Although there are situations in which inclusion of the background dielectric permittivity may be important, it has little effect on the main conclusions presented here.

Since we are interested in simulating domain patterns and polarization switching, a model for the dynamics of the polarization fields is essential. The polarization kinetics is studied within the time-dependent Ginzburg-Landau (TDGL) framework:

$$\frac{\partial P_i}{\partial t} = -\Gamma\left[\frac{\delta F_T}{\delta P_i} - E_i\right]. \quad (6)$$

Here, Γ is a kinetic coefficient related to the domain wall mobility and E_i is the component of the electric field, evaluated using Eqs. (4) and (5). We use these equations to test the stability of a single-domain remnant state as a function of the donor dopant density N_D and the thickness d and also investigate the effect of the depletion layers on polarization switching. We use natural boundary conditions $\partial P_z/\partial z = 0$ for the polarizations at the interfaces at $z = 0$ and $z = d$, which means that the interface energy does not depend on the polarization. Further, we also assume that a surface charge exactly compensates the bound surface charge due to the polarization discontinuity at the ferroelectric-electrode interfaces.

Equation (6) is discretized using finite differences. The lengths are measured in the units of the smallest length scale δ and a scaled time step of $\Delta t' = \Gamma|\alpha_1|\Delta t$.

III. STABILITY OF THE MONODOMAIN REMNANT STATE

We first address the technologically important question: How stable is a single-domain remnant state when depletion layers with free charge are present? To address this issue, we initialize the entire film in a monodomain state by setting the polarization at each point in space to $P_x = P_y = 0$ and $P_z = P_s$ (P_s is the spontaneous polarization) plus an initial noise chosen at random from the interval $\pm P_i$, where $P_i = 0.001 P_s$. The TDGL equations are integrated with short-circuit boundary conditions to study the stability of this remnant state. As discussed earlier, the depletion layer width w is described by $w = C/\sqrt{N_D}$,[17,23] where C is a property of the ferroelectric-electrode interface that depends on the built-in potential and the dielectric constant. In the present simulations, we set $C = 1.02 \times 10^5$ m$^{-0.5}$ which corresponds to a depletion layer width of $w = 16$ nm for a dopant density $N_D = 4.11 \times 10^{25}$ m^{-3}. We confirmed that choosing a larger value of C did not qualitatively change the nature of the monodomain to multidomain transitions shown in Fig. 1. We note, however, that the value of N_D at which the transition occurs does depend on the value of C. This effect is captured by the analytical solutions shown below. The TDGL simulations are performed for a series of N_D values and film thicknesses d.

At small donor dopant densities ($N_D \leqslant 5.48 \times 10^{25}$ m^{-3}), the initial single-domain state is found to be stable for all thicknesses [Figs. 1(a), 1(d), 1(g), and 1(j)]. However, for $N_D = 9.59 \times 10^{25}$ m^{-3}, the single-domain state is stable for large thicknesses [Figs. 1(b), 1(e), and 1(h)] and unstable at small thicknesses [see Fig. 1(k) for $d \leqslant 48$ nm where the film splits into a multidomain state with the formation of reverse polarization domains]. At higher values of N_D ($N_D = 11.0 \times 10^{25}$ m^{-3}), the film splits into domains at smaller thicknesses ($d \leqslant 96$ nm) [Figs. 1(f), 1(i), and 1(l)]. This shows that the monodomain to multidomain transition predicted by the present simulations can become crucial when the dopant densities are high. The appearance of this domain pattern may have important consequences for remnant polarization in ferroelectric thin films as it implies a reduction in the remnant polarization. While these results show that the remnant state is unstable with respect to the formation of reverse domains in the presence of free charge, a similar splitting of the remnant state into striped 180° domains has been predicted for films with uncompensated bound charge at electrodes.[7] However, unlike in the bound charge case, the transition observed here

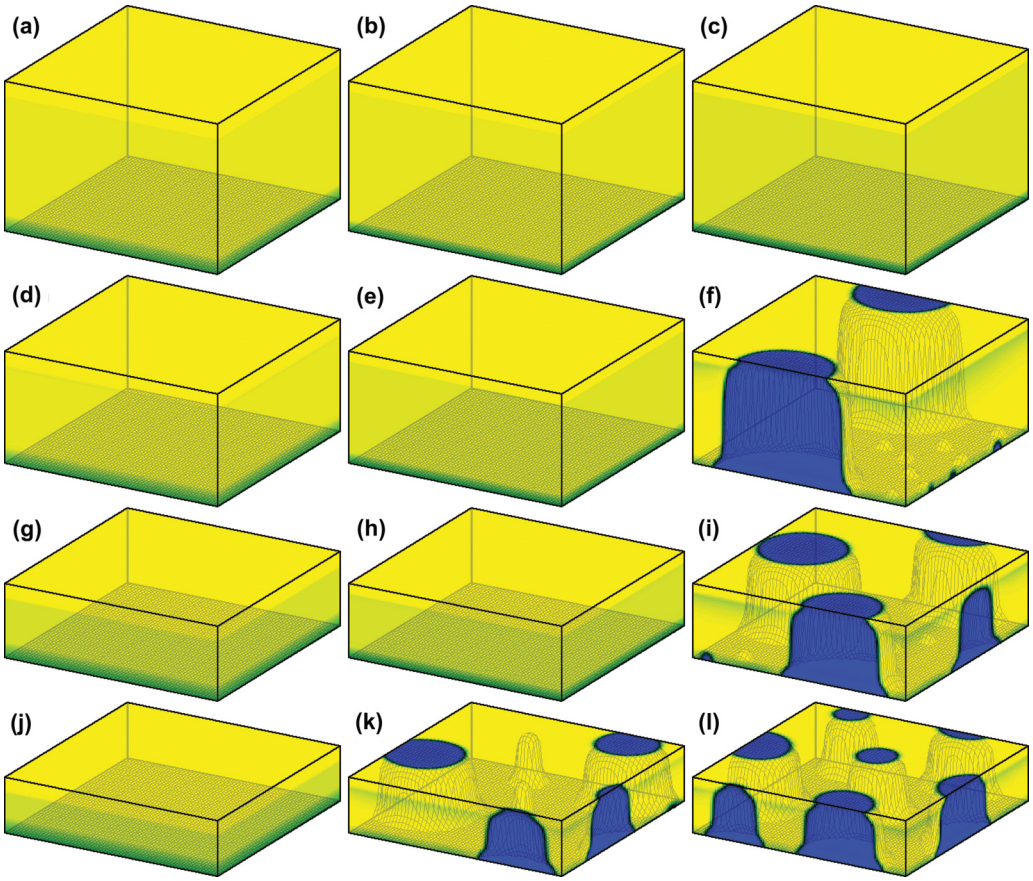

FIG. 1. (Color online) Final equilibrated domain structures from the TDGL simulation as a function of thickness (vertical axis $d = 48$, 64, 96, and 128 grid points) and donor dopant density (horizontal axis $N_D = 5.48$, 9.59, and 11.0×10^{25} m^{-3}). The depletion layer width is chosen as $w = CN_D^{-1/2}$, rounded to the nearest grid point.

is not sharp and the domain formation is localized. Depending on the value of N_D, domain formation due to depletion layer effects can be seen for thicknesses as large as ~10 times the width of the depletion layer [see Fig. 1(f)].

It is interesting to analyze the shapes of the domains observed in Fig. 1. There are two distinct kinds of domains: (i) cylindrical domains that stretch from the bottom to the top interface, expanding (flaring) into the bottom depletion layer and tapering in the top layer [Figs. 1(f), 1(i), 1(l), and 1(k)]; and (ii) domains that stretch from the bottom interface, terminating within the bulk of the film Figs. 1(f), 1(i), and 1(k)]. These domains take these shapes in order to minimize the electrostatic energy associated with charged domain walls (polarization vectors that are head to head or tail to tail). The formation of these shapes lead to rotated polarization vectors in the interfacial regions to avoid charged domain walls.

What causes the monodomain to multidomain transition? To understand this, we examined the distribution of electric fields in the film and found that a nonzero electric field, opposite to the polarization direction, exists in the bulk of the film where there is no free charge. Moreover, the magnitude of this internal electric field increases with increasing N_D and decreasing film thickness. The existence of this internal electric field and its dependence on the film thickness and the dopant density is explicitly shown in the analytical solution presented in Sec. IV. For moderate values of N_D, the internal electric field everywhere in the film is lower than the thermodynamic coercive field ($E_z > -E_c$). No domain formation occurs for these cases. However, as we consider films with higher N_D, the electric field in the bottom depletion layer approaches the thermodynamic coercive field. At a finite value of N_D, the magnitude of the electric field inside the layer exceeds the thermodynamic coercive field and domains are nucleated within the bottom depletion layers. This situation is schematically depicted in Fig. 2. Note that at the tip of these domains (for example, at point A in Fig. 2), there will be an electric field concentration (see Fig. 7) due to the depolarization fields. As N_D is increased further, the electric field concentration at the tip becomes larger than the thermodynamic coercive field (although the average electric field in the bulk regions may still be smaller). When this happens, a domain will nucleate in the bulk regions, leading to the formation of a multidomain state, similar to those in Figs. 1(f), 1(i), 1(k), and 1(l).

At this stage, some remarks on the experimental validity of this monodomain to multidomain transition are in order. The internal electric fields in perovskites for typical doping densities are much lower than the thermodynamic coercive fields. The monodomain to multidomain transition will be important when the dopant density is very high and/or for materials for which the thermodynamic coercive field is low

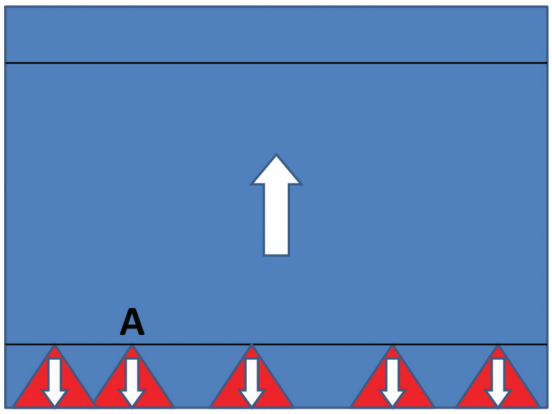

FIG. 2. (Color online) 2D schematic depicting the appearance of reversed domains inside the bottom depletion layer. Electric field concentrations at the tip of these domains (Fig. 7) can cause nucleation of domains inside the bulk of the film where there is no depletion charge.

(e.g., at temperatures close to the second-order transition points). Even for the cases where the built-in electric field is low, the presence of defects may still lead to the nucleation of reverse domains.

IV. ONE-DIMENSIONAL ANALYTICAL SOLUTION

The basic physics associated with three-dimensional (3D) simulation results can be deduced from a simplified one-dimensional model. An analytical solution for the electric field distribution inside films with depletion layers was obtained by Tagantsev *et al.*[17] for the special case of a linear dielectric material. Here we derive an analytical solution that takes into account the nonlinearity of the dielectric constant—an important feature of ferroelectrics. We start with the Landau free energy (to fourth order in the polarization):

$$F_T = \tfrac{1}{2}\alpha_1 P_z^2 + \tfrac{1}{4}\alpha_{11} P_z^4, \tag{7}$$

and the appropriate electric field,

$$E_z = \frac{\partial F_T}{\partial P_z} = \alpha_1 P_z + \alpha_{11} P_z^3. \tag{8}$$

Next, we rewrite Gauss's Law as $\varepsilon_0 \frac{\partial E_z}{\partial P_z}\frac{\partial P_z}{\partial z} + \frac{\partial P_z}{\partial z} = \rho(z)$, or $\frac{\partial P_z}{\partial z} = \rho(z)[1 + \varepsilon_0 \frac{\partial E_z}{\partial P_z}]^{-1}$. Since χ is large in ferroelectrics, $1/\chi = \varepsilon_0(\partial E_z/\partial P_z) = \varepsilon_0[\alpha_1 + 3\alpha_{11}P_z^2]$ is small. Taylor-expanding to first order in $\varepsilon_0(\partial E_z/\partial P_z)$ we can write

$$\frac{\partial P_z}{\partial z} = \rho(z)\left[1 - \varepsilon_0 \frac{\partial E_z}{\partial P_z}\right]. \tag{9}$$

Integrating Eq. (9) in the depletion layers and setting $P_z = P_b$ for $w < z < d - w$, we find

$$P_z = \begin{cases} a\tanh\{b\rho_0(z-w)\} + P_b, & z < w \\ P_b, & w < z < d-w, \\ a\tanh\{b\rho_0[z-(d-w)]\} + P_b, & z > d-w \end{cases} \tag{10}$$

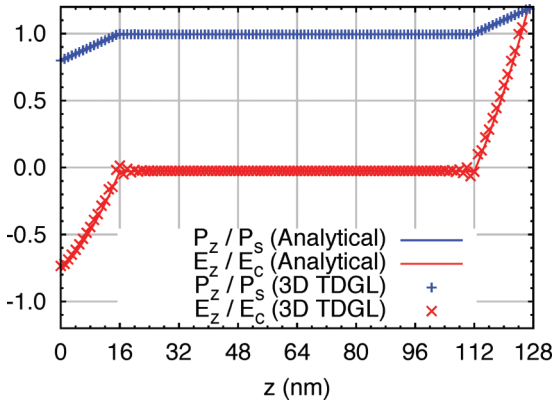

FIG. 3. (Color online) Polarization and electric field profiles: P_z/P_s and E_z/E_c versus z ($N_D = 2.74 \times 10^{25}$ m^{-3}) obtained from the analytical solution as compared to the 3D simulation with the same fourth-order Landau parameters.

Where $a = \sqrt{(1-\alpha_1\varepsilon_0)/(3\alpha_{11}\varepsilon_0)}$, $b = \sqrt{3\alpha_{11}\varepsilon_0(1-\alpha_1\varepsilon_0)}$, and P_b represents the polarization in the bulk of the film where there is no free charge. P_b can be computed by applying the boundary condition, $-U = \int_0^d E_z dz$, where $-U/d = E_{\text{ext}}$ is the contribution from the external electric field. Using (8) and (10) we obtain the renormalized equations from which the effective hysteresis loop for the film can be expressed as

$$E_{\text{ext}} = \tilde{\alpha}_1 P_b + \alpha_{11} P_b^3, \tag{11}$$

where

$$\tilde{\alpha}_1 = \left\{\alpha_1 + 2\frac{w}{d}\left(\frac{1}{\varepsilon_0} - \alpha_1\right)\left[1 - \frac{\tanh(b\rho_0 w)}{b\rho_0 w}\right]\right\}. \tag{12}$$

The combined effects of space charge and thickness are to simply shift the effective value of α_1. Here, P_b can be obtained using the standard solution for a cubic equation. Under zero external field, $P_b = \pm\sqrt{-\tilde{\alpha}_1/\alpha_{11}}$, i.e.,

$$\frac{P_b}{P_s} = r = \pm\sqrt{1 - 2\frac{w}{d}\left[1 - \frac{1}{\alpha_1\epsilon_0}\right]\left[1 - \frac{\tanh(b\rho_0 w)}{b\rho_0 w}\right]} \tag{13}$$

where $P_s = \sqrt{-\alpha_1/\alpha_{11}}$ is the spontaneous polarization for the film without depletion layers. The corresponding bulk electric field, E_b, is calculated using $E_b = \alpha_1 P_b + \alpha_{11} P_b^3$ as

$$E_b/E_c = \mp\frac{3\sqrt{3}}{2} r(1 - r^2), \tag{14}$$

where E_c is the intrinsic (thermodynamic) coercive field of the film without depletion layers.

Combining Eqs. (10) and (13), we obtain a closed form expression for the polarization profile, $P_z(z)$, that includes the effects of both space charge and thickness dependence. Substitution into Eq. (8), $E_z = \alpha_1 P_z + \alpha_{11} P_z^3$, yields an explicit formula for the electric field profile.

The profiles of P_z and E_z have been validated against the 3D TDGL simulations as shown in Fig. 3. This agreement holds even though the analytical solution ignores the value of the gradient coefficient, K. Since the length scale of our

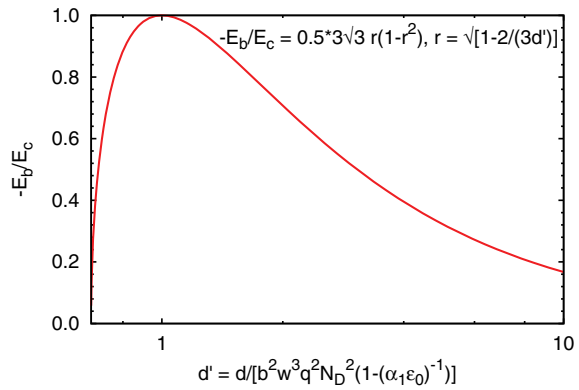

FIG. 4. (Color online) Rescaled internal electric field, $-E_b/E_c$, versus rescaled film thickness d'.

simulation is set by our choice: $K' = K/(|\alpha|\delta^2) = 1.0$, where K' is inversely proportional to δ^2, it is believed that this agreement will hold even if the length scale $\delta = 1$ nm is changed, meaning that our results should hold if we rescale our simulation (by changing δ) within reasonable limits. Note also that since the analytical solution has been obtained using fourth-order Landau theory, we have appropriately chosen the parameters such that the equilibrium polarization is the same as the full eighth-order expansion considered in the 3D simulations of Fig. 1. For typical values of N_D (such as those used by Zubko *et al.*[16]), we can expand the hyperbolic tangent term in Eq. (13) in a Taylor series. Truncating at fourth order gives

$$\frac{P_b}{P_s} = r \cong \pm\sqrt{1 - \frac{2}{3}\frac{b^2 w^3 q^2 N_D^2}{d}\left[1 - \frac{1}{\alpha_1 \epsilon_0}\right]}. \quad (15)$$

From this analysis, we see that a nonzero electric field E_b exists (except in the $w/d \to 0$ or $\rho_0 \to 0$ limits where $|P_b| = P_s$) even for short-circuit boundary conditions ($E_{ext} = 0$). The nonzero E_b explains the internal electric field observed in the 3D simulations (Fig. 3). Examination of Eqs. (14) and (15) suggests that it is useful to introduce a dimensionless distance:

$$d' = \frac{d}{b^2 w^3 q^2 N_D^2 [1 - (\alpha_1 \varepsilon_0)^{-1}]}. \quad (16)$$

By substituting $w = C/\sqrt{N_D}$ into Eq. (16), we see that the key parameter that determines the scaling of the bulk polarization P_b/P_s or the bulk electric field E_b/E_c is $d/N_D^{1/2}$ or dw.

How does the internal electric field, E_b, vary with the film thickness and the dopant density? To address this, we plot (see Fig. 4) E_b versus the rescaled thickness, d', obtained from the analytical solution [Eqs. (14) and (15)]. Clearly, the magnitude of the internal electric field increases with decreasing d' until $d' = 1$, where the bulk electric field, E_b, becomes equal to the intrinsic coercive field. In a full 3D simulation, this large internal field in the bulk and depletion layers leads to the monodomain to multidomain transition that was observed in Figs. 1(f), 1(i), 1(k), and 1(l). Note that the film actually splits into a multidomain state well before $|E_b/E_c| = 1$, as $|E_z/E_c|$ at $z = 0$ reaches the coercive field for switching earlier than $|E_b/E_c|$ (see Fig. 3).

We can draw useful conclusions about the thickness dependence and dopant density dependence of the internal electric field by examining Fig. 4, which clearly shows that for a fixed value of the dopant density N_D, the internal electric field increases with decreasing film thickness d. Figure 4 also shows that for a fixed thickness d, the magnitude of the internal electric field increases with increasing dopant density N_D. As discussed in Sec. III, this behavior is indeed observed in the 3D simulations (Fig. 1); the internal electric field is the key to explain the monodomain to multidomain transition.

V. INFLUENCE OF THE DEPLETION LAYERS ON POLARIZATION SWITCHING

Does the depletion layer play any role during the polarization switching process? Recently, Zubko *et al.*[16] studied the influence of depletion layers on hysteresis loops in thin films using a 1D Ginzburg-Landau model. In their monodomain study, they found that the depletion layers both tilt and shrink the hysteresis loops. This theoretical study[16] did not include effects associated with domain structure evolution during the switching process. We simulate the evolution of domain patterns under an applied external field by applying a time-dependent (sawtooth with a 1.6×10^6 time step switching period) potential to each of the domain structures shown in Fig. 1. Before we describe our results on the polarization switching behavior, we remark that we are using a frozen depletion layer approximation (i.e., the depletion layer width does not change appreciably during polarization switching). This is a reasonable approximation for polarization switching that occurs quickly relative to any change in charge carrier profile. For example, domain wall velocities in $BaTiO_3$ can be in the 10^{-7}–10^5 cm/s range, depending on the electric field.[26–29] This should be compared with the speed of oxygen vacancies; multiplying the oxygen vacancy drift mobility of 8.4×10^{-22} m^2/(V s) (Ref. 20) by the intrinsic coercive field of $BaTiO_3$ [126 MV/m (Ref. 30)] we find an oxygen vacancy velocity of 1.06×10^{-13} m/s. Since the velocity of the oxygen vacancies is much, much smaller than domain wall velocities, it is appropriate to conclude that the depletion layer thickness does not significantly change during polarization switching at typical switching frequencies. Hence, the frozen depletion layer approximation should be valid here. On the other hand, if the mobile charges are primarily electrons and holes, or if we consider extremely low switching frequencies (of the order of the oxygen vacancy velocity, the results in Fig. 5 should be viewed only as qualitative).[31]

Figure 5 shows the simulated hysteresis loops for films with $d = 64$ and 128 nm, along with the corresponding thermodynamic switching loop obtained from the homogeneous Landau theory (in the absence of the depletion layers). Note that the coercive field is lower than the thermodynamic coercive field, E_c, for both thicknesses. This is associated with the internal electric field E_b which opposes the polarization and aids the switching process. Since $|E_b|$ increases with decreasing thickness (Fig. 4), the coercive field decreases with decreasing thickness. We also find that the switching process is inhomogeneous; it occurs via domain nucleation and growth. Figures 5(a)–5(d) depict this process for the $d = 64$ nm film. Nucleation of reverse domains occurs where

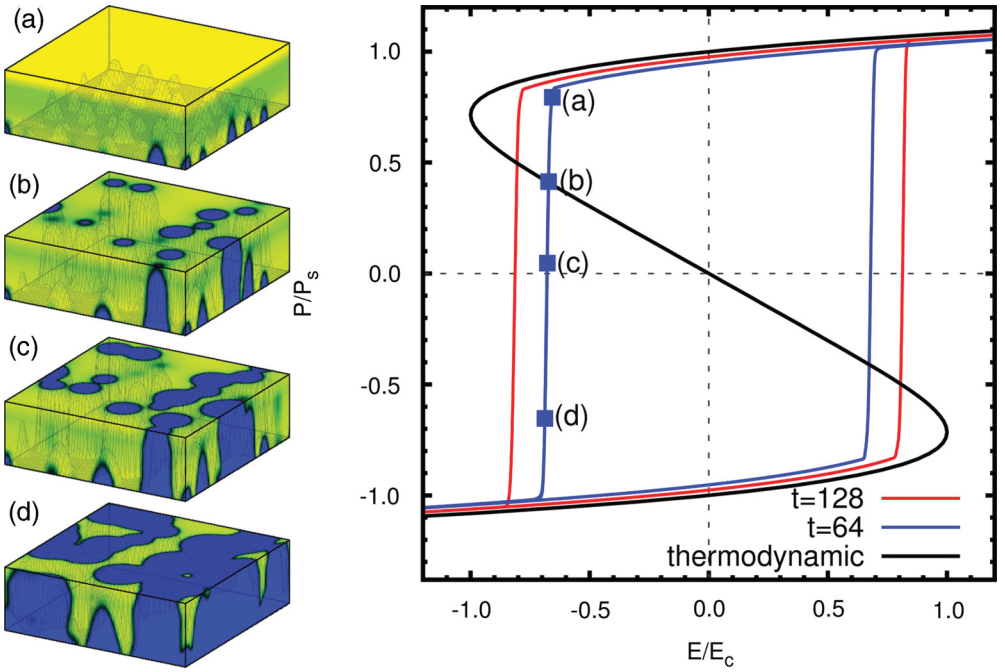

FIG. 5. (Color online) Hysteresis loops for $N_D = 4.11 \times 10^{25}$ m^{-3}, $d = 64$, 128 nm. The domain patterns corresponding to points (a)–(d) for the $d = 64$-nm film are also shown. The video for nucleation and growth of domains through points (a)–(d) is provided in the Supplemental Material (Ref. 32).

E_z is most negative, i.e., at the bottom electrode ($z = 0$) once $|E_z|_{z=0} > E_c$ as predicted by Ref. 2. While many small reverse domains nucleate during the switching process, the larger reverse domains grow and nearby smaller reverse domains disappear. It is interesting to note that in our model the positions of the reverse domains are random, and come from the thermal noise that we introduce into our model—we do not introduce any nuclei of reversed polarization or charged defects. The nucleated reverse domains grow by lateral domain wall migration and coalescence. At sufficiently high electric field, the polarization in the entire film reverses. Thus, we observe that the depletion layers have significant influence on the polarization switching process.

The shapes of reverse domains formed during the switching process are similar to those observed in Fig. 1 under short-circuit boundary conditions. To understand these domain shapes, it is instructive to examine the distributions of polarization and electric field in the vicinity of a reverse domain for a domain formed during the polarization switching process. Figure 6 shows the polarization vectors near the domain wall

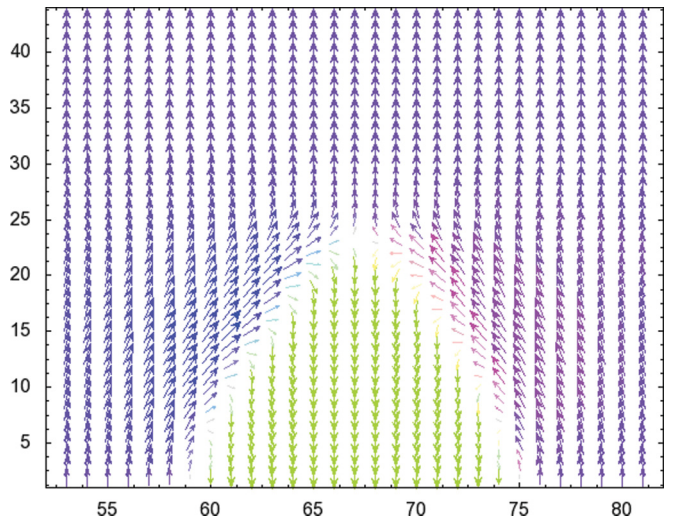

FIG. 6. (Color online) The polarization vectors in the vicinity of a conical reverse domain in the ferroelectric film near the lower contact. Note the rotation of the polarization vectors near the domain wall. Arrows are blue for $P_z > 0$ and yellow for $P_z < 0$.

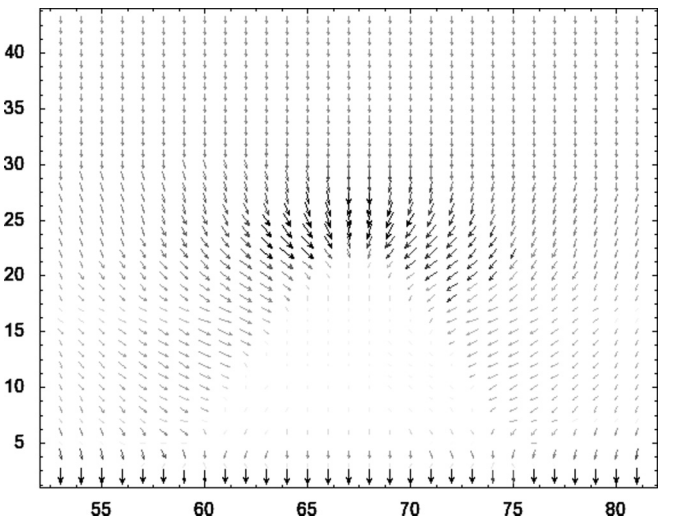

FIG. 7. Electric field vectors corresponding to the domain wall configuration in Fig. 6. The electric field is strongest in the vicinity of the tip of the reverse domain (where polarization vectors are tail to tail) and weakest in the interior of the reverse domain.

are approximately parallel to the wall. The electrostatic energy of the domain walls is large where the polarization vectors are head to head or tail to tail. Hence, these vectors rotate along the entire domain wall except at the tip of the reverse domain, where the electric field is the strongest (see Fig. 7). The rotated polarization vectors screen the electric field, and in the interior of the reverse domain, the electric field is effectively zero (Fig. 7). However, the magnitude of the electric field is approximately equal to the intrinsic coercive field, E_c, in the original domain immediately above the tip of the reverse domain.

VI. SUMMARY AND CONCLUSION

In summary, using 3D phase field simulations we show that depletion layers at the ferroelectric thin film/electrode interface can create an internal electric field in the bulk regions where there is no free charge. This is also demonstrated explicitly through an analytical solution of a 1D Ginzburg-Landau model with depletion layers. We show that this internal electric field can have very important implications for thin-film ferroelectrics. At high values of the donor dopant density and at thicknesses which are comparable to depletion layer width, a single-domain remnant state can become unstable due to the appearance of a domain pattern. A multidomain state with conical and cylindrical 180° domains (Fig. 1) is observed for such cases, resulting in a significant drop in the value of the remnant polarization. Further, it is found that the depletion layers also play an important role in domain nucleation during polarization switching. The phenomena reported in the present paper are distinct from those that are observed due to depolarization fields from uncompensated surface charges. While the depolarization fields due to bound charges become important only for very small thicknesses, the internal electric field due to depletion layers predicted by our calculations may become important for relatively thicker films, depending on the dopant density and the choice of the electrode.

[1] C. Lichtensteiger, M. Dawber, and J.-M. Triscone, Top. Appl. Phys. **105**, 305 (2007).

[2] A. K. Tagantsev and G. Gerra, J. Appl. Phys. **100**, 051607 (2006).

[3] A. M. Bratkovsky and A. P. Levanyuk, Phys. Rev. Lett. **84**, 3177 (2000).

[4] M. Marvan and J. Fousek, Phys. Status Solidi B **208**, 523 (1998).

[5] R. R. Mehta, B. D. Silverman, and J. T. Jacobs, J. Appl. Phys. **44**, 3379 (1973).

[6] M. Dawber, P. Chandra, P. B. Littlewood, and J. F. Scott, J. Phys.: Condens. Matter **15**, L393 (2003).

[7] A. M. Bratkovsky and A. P. Levanyuk, Appl. Phys. Lett. **89**, 253108 (2006).

[8] G. Gerra, A. K. Tagantsev, and N. Setter, Phys. Rev. Lett. **98**, 207601 (2007).

[9] J. Junquera and Ph. Ghosez, Nature **422**, 506 (2003).

[10] G. Gerra, A. K. Tagantsev, N. Setter, and K. Parlinski, Phys. Rev. Lett. **96**, 107603 (2006).

[11] R. Ahluwalia and D. J. Srolovitz, Phys. Rev. B **76**, 174121 (2007).

[12] D. Damjanovic. Rep. Prog. Phys. **61**, 1267 (1998).

[13] Y. Xiao, V. B. Shenoy, and K. Bhattacharya, Phys. Rev. Lett. **95**, 247603 (2005).

[14] A. M. Bratkovsky and A. P. Levanyuk. Phys. Rev. B **61**, 15042 (2000).

[15] L. Baudry and J. Tournier, J. Appl. Phys. **97**, 024104 (2005).

[16] P. Zubko, D. J. Jung, and J. F. Scott, J. Appl. Phys. **100**, 114112 (2006).

[17] A. K. Tagantsev, Cz. Pawlaczyk, K. Brooks, and N. Setter, Integr. Ferroelectr. **4**, 1 (1994).

[18] A. N. Morozovska, E. A. Eliseev, S. V. Svechnikov, A. D. Krutov, V. Y. Shur, A. Y. Borisevich, P. Maksymovych, and S. V. Kalinin, Phys. Rev. B **81**, 205308 (2010).

[19] E. A. Eliseev, A. N. Morozovska, G. S. Svechnikov, V. Gopalan, and V. Y. Shur, Phys. Rev. B **83**, 235313 (2011).

[20] Y. A. Genenko, Phys. Rev. B **78**, 214103 (2008).

[21] N. A. Pertsev, A. G. Zembilgotov, and A. K. Tagantsev, Phys. Rev. Lett. **80**, 1988 (1998).

[22] Y. L. Li, L. E. Cross, and L. Q. Chen, J. Appl. Phys. **98**, 064101 (2005).

[23] S. M. Sze and K. K. Ng, *Physics of Semiconductor Devices*, 3rd ed. (Wiley, Hoboken, NJ, 2007).

[24] V. B. Shenoy, Y. Xiao, and K. Bhattacharya, J. Appl. Phys. **111**, 084105 (2012).

[25] J. Hlinka and P. Marton, Phys. Rev. B **74**, 104104 (2006).

[26] H. L. Stadler and P. J. Zachmanidis, J. Appl. Phys. **34**, 3255 (1963).

[27] Robert C. Miller and Gabriel Weinreich, Phys. Rev. **117**, 1460 (1960).

[28] M. Hayashi, J. Phys. Soc. Jpn. **34**, 1240 (1973).

[29] J. F. Scott, F. D. Morrison, M. Miyake, P. Zubko, X. Lou, V. M. Kugler, S. Rios, M. Zhang, T. Tatsuta, O. Tsuji, and T. J. Leedham, J. Am. Ceram. Soc. **88**, 1691 (2005).

[30] The intrinsic coercive field based on the coefficients of Eq. (2) is 15 MV/m, but the compressive strain rescales these coefficients to give a larger intrinsic coercive field.

[31] Even if the majority charge carriers are electrons/holes, the following observations still pertain: (i) The coercive field decreases with increasing N_d [as observed by Zubko *et al.* (Ref. 16)]; (ii) the reverse domains grow from the depletion layer where the magnitude of the polarization is lower than the bulk of the film, expand through the film, and taper into the depletion layer at the opposite side of the film (the shapes of the reverse domains are as shown in Figs. 1 and 5); and (iii) the electric field distributions around the growing reverse domains are qualitatively similar to those shown in Fig. 7.

[32] See Supplemental Material at http://link.aps.org/supplemental/10.1103/PhysRevB.86.094104 for a movie of the switching process.